CZECH TECHNICAL UNIVERSITY IN PRAGUE

Faculty of Civil Engineering
Department of Mechanics

Combination of homogenization and nanoindentation in search for microfibril angle of spruce

Bachelor Thesis

Study Programme: Civil Engineering (Czech)
Branch of study: Building Structures (Czech)

Thesis advisor: Prof. Ing. Michal Šejnoha, Ph.D., DSc.

Lucie Kucíková

Prague 2016

ZADÁNÍ BAKALÁŘSKÉ PRÁCE

I. OSOBNÍ A STUDIJNÍ ÚDAJE

Příjmení: Kucíková   Jméno: Lucie   Osobní číslo: 412638

Zadávající katedra: K132 - Katedra mechaniky

Studijní program: SI - Stavební inženýrství

Studijní obor: C - Konstrukce pozemních staveb

II. ÚDAJE K BAKALÁŘSKÉ PRÁCI

Název bakalářské práce: Kombinace homogenizace a nanoindentace pro odhad úhlu mikrofibril smrkového dřeva

Název bakalářské práce anglicky: Combination of homogenization and nanoindentation in search for microfibril angle of spruce

Pokyny pro vypracování:
- v anglickém jazyce

Seznam doporučené literatury:
M. Šejnoha, J. Zeman: Micromechanics in Practice

Jméno vedoucího bakalářské práce: Prof. Ing. Michal Šejnoha, Ph.D., DSc.

Datum zadání bakalářské práce: 25.2.2016   Termín odevzdání bakalářské práce: 20.5.2016

_____   _____
Podpis vedoucího práce   Podpis vedoucího katedry

III. PŘEVZETÍ ZADÁNÍ

Beru na vědomí, že jsem povinen vypracovat bakalářskou práci samostatně, bez cizí pomoci, s výjimkou poskytnutých konzultací. Seznam použité literatury, jiných pramenů a jmen konzultantů je nutné uvést v bakalářské práci a při citování postupovat v souladu s metodickou příručkou ČVUT „Jak psát vysokoškolské závěrečné práce" a metodickým pokynem ČVUT „O dodržování etických principů při přípravě vysokoškolských závěrečných prací".

25.2.2016
_____   _____
Datum převzetí zadání   Podpis studenta(ky)

Declaration of authorship

Hereby I declare that I have completed Bachelor thesis called "*Combination of homogenization and nanoindentation in search for microfibril angle of spruce*" by myself. Used literature and other references are mentioned in the References.

In Prague, May 20th, 2016   ……………………………….

Acknowledgements

Contents

Abstract

Topic: Combination of homogenization and nanoindentation in search for microfibril angle of spruce

The thesis is concerned with the estimation of the microfibril angle in the wood cell wall using the combination of the micromechanical homogenization and nanoindentation measurement. For the homogenization, the upscale model was used employing the Self-consistent method for the first step (Polymer network) and the Mori-Tanaka method for the second (Cell wall) and the third one (Lumens), and also the standard rule of mixtures for the fourth step (Laminate). The effective longitudinal elastic modulus of the cell wall level with rotated microfibrils was compared with Young's modulus from the nanoindentation. This iterative computation led to the microfibril angle (MFA).

Keywords: homogenization, MFA, spruce, wood, nanoindentation, orientation averaging, Mori-Tanaka method, self-consistent method

Abstrakt

Téma práce: Kombinace homogenizace a nanoindentace pro odhad úhlu mikrofibril smrkového dřeva

Tato práce se zabývá odhadem odklonu celulózových vláken v buněčné stěně smrkového dřeva využitím porovnání výsledků získané mikromechanickou homogenizací s výsledky měření pomocí nanoindentace. Homogenizace byla prováděna s postupným zvětšováním měřítka tzv. "od nejmenšího k největšímu" pomocí self-konzistentní metody pro první stupeň (polymerní síť), metody Mori-Tanaka pro druhý (buněčná stěna) a třetí stupeň (lumeny) a pomocí klasické laminační teorie pro čtvrtý stupeň (laminát). Následně postupným porovnáváním efektivního modulu pružnosti, získaného homogenizací na úrovni buněčné stěny s různě natočenými vlákny, a Youngova modulu pružnosti z měření pomocí nanoindentace byl zjištěn výsledný odklon mikrofibril.

Klíčová slova: homogenizace, odklon mikrofibril, smrk, dřevo, nanoindentace, orientační průměrování, metoda Mori-Tanaka, self-konzistentní metoda

1. Introduction

The wood is a natural material used as a building material for thousands years, however this material is not known enough. In these times, when all environmentally friendly things are very popular, wood became "in" and wood industry is flourishing. That's because it is a renewable source, comparing to, e.g. cement, which is totally non-renewable. There are much more advantages, e.g. trees produce oxygen, the natural biotope remains to wild animals etc. Also using wood in interiors makes people feel comfortable and warm-in-heart.

Almost 36,8 % of the Czech Republic [9] land is covered by forests. Naturally, wood is one of the mainly used building materials. The most cultivated wood species is the Norway spruce (*Picea abies*), which belongs to conifers. In the Czech Republic the spruce is a major constituent of the timber production – almost 80 % of the whole production [10].

2. Wood structure

Tree stem is mainly used for timber industry, when it is cut into boards, beams etc., so only properties of the tree stem are considered. Wood, generally, has a highly irregular structure depending on growth conditions, e.g. location, age of the tree, climate, weather etc. It is possible to determine wood as a fibre reinforced polymer composite. In the following, the structure is described from macrostructure, which can be seen by naked eye, to ultrastructure, visible using microscope with high resolution only.

2.1 Macrostructure

The macrostructure of wood is discernible by naked eye. Outermost part is a bark, which is like a skin for the tree. Protects it against injuries, microbial attacks and other harmful agents. Below bark is phloem also called inner bark, which new bark layers come from. Next is cambium, the most important layer of the whole tree, where new cells are produced (cell production and cell division is not a case of this study, for more information see [1]). The main mass of the wood stem is xylem, where one layer produced by cambium in one growing season is called growth ring or annual ring. In the xylem growth rings appear as darker (latewood) and lighter (earlywood) lines, which make almost circles around the middle of the stem. Perpendicularly to growth rings run rays in radial directions, some starting from the pith and some from heartwood or sapwood.

In the middle of the stem is a darker zone called pith, which comes from the very beginning of a tree life. The first several growth rings are also called juvenile wood, which is dated to the time, when the tree was a small sapling. Another possible division of the xylem is into sapwood and heartwood. Sapwood contains live cells, while all cells are "dead" in the heartwood, it means that all pit pairs are closed and could not conduct water and nutrients [1]. Fig. 1 illustrates schematically this structural composition.
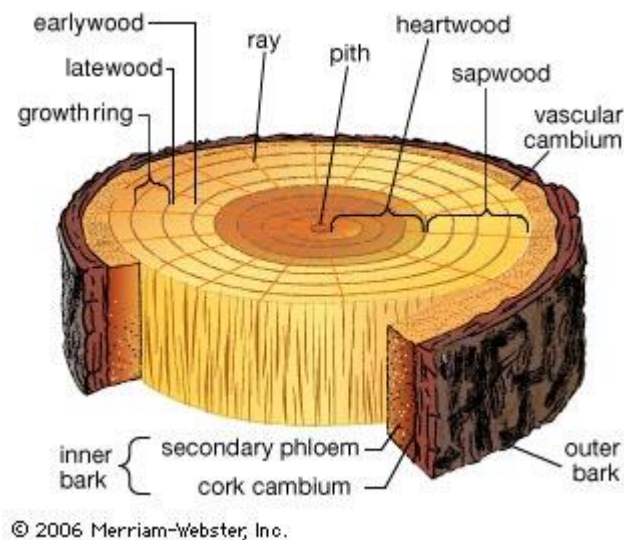

Fig. 1 Wood macrostructure [2]

The width of the growth ring is highly dependent on growing conditions, such as temperature distribution during the season, precipitation amount, growth place etc. The lower temperature is, the thinner is the growth ring and the higher is the density of wood. This predetermines the wood from northern parts as a material with better mechanical properties compared to the wood from southern parts.

Another characteristic, which affects the final properties, is the amount of knots and other inhomogeneities, such as animal bite or ingrown bark. Knots are the remnants of branches, which were cut off during logging or broken when they died. There are two types of knots. The first one originate from living branches and the second one are residues of the dead branches over which the stem grew. These are called internal knots. In a knot and around it, the orientation of the cells deviates from that in the main stem, so it causes a local concentration of lower properties, which results into the knot density dependence of the strength properties of the wood. Due to its higher density, it shrinks more than the surrounding wood and usually falls out [1].

When the growth rings seem to be non-central, it usually points to the stem under stress. The wood under stress is called reaction wood and divides into two main groups:

compression wood and tension wood. The tension wood develops in parts under tension. The annual rings are thicker and lighter in colour, with higher tensile strength, which could be caused by lower microfibril angle. Also, the content of main cell wall constituents is different than in the normal wood. The cell walls exhibit more cellulose and less lignin. While the compression wood, which develops under compression stress, is almost the opposite. The growth rings are thinner and darker in colour, with shorter and round in cross-section tracheids, which exhibit higher microfibril angle. Cracks appear on the inner side of the cell wall and extend quite deep into the S2 layer, while S3 layer is completely absent. The compression wood contains less cellulose and more lignin than the normal wood and exhibits higher compression strength and higher ductility. The reaction wood is usually eliminated from the timber production due to its shape changes [1].

2.2 Microstructure

Wood, as many biological materials, consists of several types of cells, which are produced in cambium. Spruce, which belongs to conifers (softwood), mainly consists of tracheids, approximately 94% of the wood volume. The microstructure is depicted on Fig.2 and 3.

Tracheids are long closed tube-like cells with almost rectangular cross section, elongated in the axial direction of the stem. The void inside a cell is called lumen and serve as a conductor of water and nutrients. In the longitudinal direction, they are joined to one another finger-like and the water and nutrients run through the pit pairs (see Fig. 3), possibly described as small holes in the cell wall of each attached cell. In the radial and tangential direction, cells are joined together by middle lamella, acting as a "glue" between cells. The length is about 2,5 – 2,82 mm and width about 13 – 39,3 µm (depending on the cell type and direction), approximately, so the value of the length over thickness ratio is about 100:1. There are obvious differences between earlywood and latewood tracheids. Earlywood tracheids have thinner walls and bigger lumens, because they are mainly used for conduction in the beginning of the growing season. Unlike them, latewood tracheids are much thicker with small lumens, used as a storage area and mechanical support of a crown. Also the cross section is different, for earlywood is typical almost square shape, contrary to latewood, which is more rectangular. In the tangential direction almost all cells have the same width, however in the radial direction, latewood cells are nearly half in width [1].

Another type are parenchyma cells, which are almost the same as tracheids, except for the length and different type of pits. In the spruce, they mostly appear as building parts of rays and resin canals.
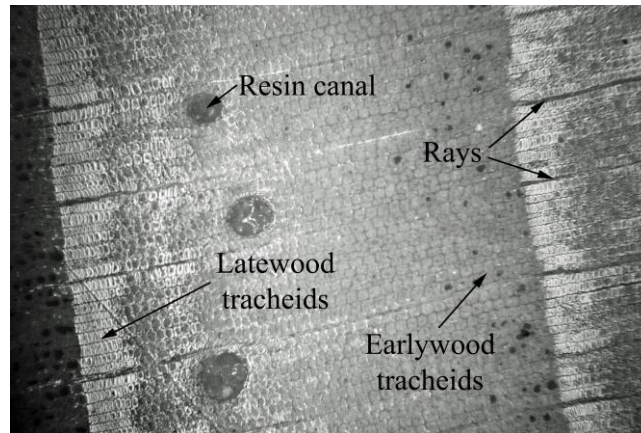

Fig. 2 Microstructure of the spruce (optical microscope) – cross section

There are also cells oriented radially comprising tracheids and parenchyma cells. This structure is called ray and is made of a group of cells together, starting from pith or heartwood and sapwood. Rays work as conductors in the radial direction of the stem. Because of this purpose, they are connected one to another and also with axial tracheids. In the cross section, they appear as tube-like lines (Fig. 2) and in the longitudinal section as a group of cells. In a case of the spruce the ray is one cell wide and a few cells high, see Fig. 3. The volume fraction of rays is 5,9%, approximately [1].

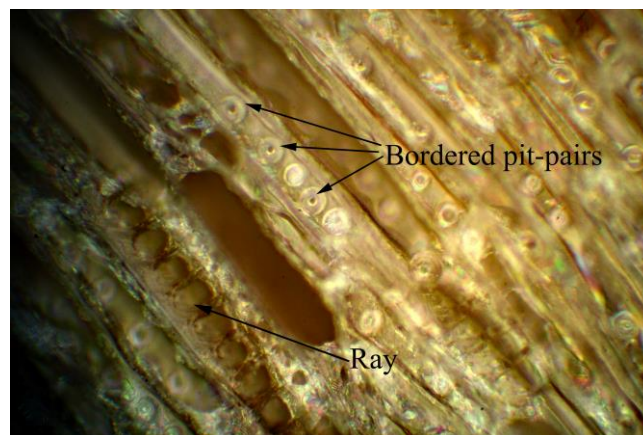Fig. 3 Microstructure of the spruce (optical microscope) – tangential direction

Next microstructure appearing in wood is a resin canal (Fig. 2). This structure occurs in both longitudinal and radial direction as a huge hole surrounded by some cells. Resin canals serve as resin conductors running through the whole tree. The amount of the resin canals is small, approximately 0,14% of the wood mass [1].

2.3 Ultrastructure

When the structure of the wood is studied with larger magnification, e.g. the polarised light microscope, the cell wall appears to be composed of several layers, so it is possible to determine cell wall as a multilayer laminate. As it is evident from Fig. 4 the layers are (described outwards): warty layer, secondary wall, primary wall and middle lamella (sometimes called intercellular layer).
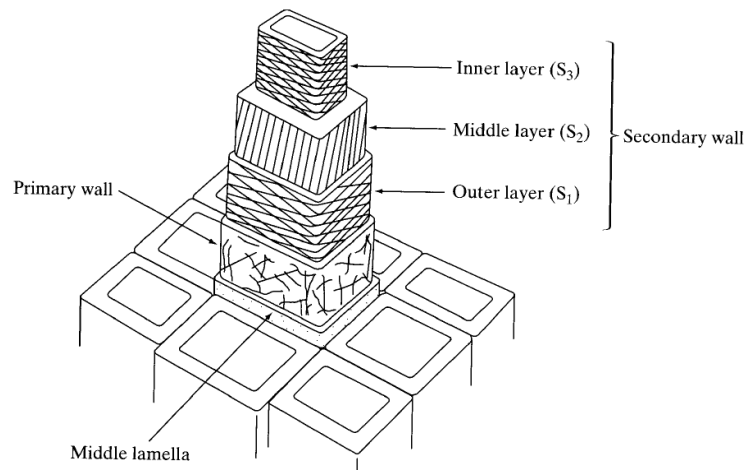

Fig. 4 The structure of the tracheid cell wall and middle lamella [1]

The warty layer is a continuous thin amorphous layer containing some fibres and warts. This layer is not found in all wood species, but softwood tracheids have it nearly always.

The secondary wall consists of several layers. The main division is into three layers: outer layer S_1, middle layer S_2 and inner layer S_3. The outer layer S_1 is composed of several lamellae with cross fibrillary texture, which means that the direction of the reinforcing fibres in reference to the axial direction alternate left to right with relatively wide angle, see Fig. 4. Its thickness is about $10 - 15\%$ of the total thickness of the secondary wall. The middle layer S_2 is the thickest layer compared to S_1 and S_3 covering about 85% of the total thickness of the secondary wall. There is a small deviation of the reinforcing fibres from the longitudinal axis and a high degree of parallelism of microfibrils (the cellulose fibres). The middle layer has a great influence on the properties of the cell wall and subsequently on the properties of the whole stem. The inner layer S_3 has similar structure as outer layer, with higher deviation of the fibres from axial direction. There are also transition lamellae with a gradual shift of microfibril

angles (the deviation of the cellulose fibres from the longitudinal axis) between S_1 and S_2 and between S_2 and S_3.

The primary wall is the first cell wall layer produced in the cambium, this is the reason of the imperfection of this layer. It consists of a single lamina with more or less randomly oriented microfibrils. Microfibrils will be mentioned in Section 5.

The middle lamella joins the cells together. It is totally amorphous, highly lignified material without any reinforcement. Due to the lack of the reinforcement and amorphous structure, the middle lamella is weaker than the cell wall [1, 3].

The wood cell walls consist mainly of cellulose (predominantly crystalline), hemicellulose (predominantly amorphous) and lignin (totally amorphous). Apart from these basic components, other substances appear in the wood microstructure, such as extractives, water and some additional minor components.

The cellulose ($C_6H_{10}O_5$) is a semi-crystalline thermoplastic natural polymer forming the reinforcing microfibers in the cell wall. Cellulose is produced by polymerization of glucose monomers into a linear molecule chain. The molecule chains can form larger units, crystalline or amorphous in arrangement (crystalline and amorphous cellulose mentioned in Section 4 in the second step of homogenization). Hemicelluloses are heteropolysaccharides composed of glucose and other monomers, e.g. mannose, galactose, xylose, arabinose and others. They have semi-crystalline structure with a dominant amorphous structure component. Lignin is a large molecule composed of phenyl propane units where hydroxyl- and methoxy- groups substitute hydrogen. It has a very complicated and heterogeneous structure. There are many types of lignin, differing due to its location. The main task of lignin is to act as a "glue" between macrofibrils (units composed of cellulose microfibrils and hemicellulose layers around them) [1].

3. Nanoindentation

3.1 Main principle

The nanoindentation is usually used for elastic modulus and hardness measurements at the micrometre and nanometre scales. The main principle is pushing of small hard tip with known geometry and material properties to a material with unknown properties. During the indentation, loading force and displacement of the tip are measured and the dependence of these parameters is depicted by load-displacement curve, see Fig. 5,

where P_{max} is the maximum load, h_{max} is the maximum displacement, S=dP/dh is the elastic unloading stiffness defined as the slope of the unloading curve and h_f is the final depth, the permanent depth of penetration after the indenter is fully unloaded. In this thesis, the Berkovich tip – the sharp, geometrically self-similar triangular pyramid made of diamond, was used for the static indentation on Hysitron® TI 750L Ubi™.

During loading the elastic and plastic deformation is assumed, whereas only elastic deformation is supposed to be during unloading. The maximum force holding is used to ensure that only elastic deformation appears and the viscoelastic material response is eliminated, this is very important in the case of wood, because it exhibits viscoelasticity. The properties of the tested material are computed from the unloading part of the load-displacement curve obtained during one cycle of loading and unloading; basic equations of the isotropic indentation are mentioned in section 3.2 assuming the isotropic half space [4].

Fig. 5 Load-displacement curve and unloading process of the indenter tip [4]

3.2 Basic equations for static isotropic nanoindentation

Contact depth

Assuming that the pile-up is negligible, which actually isn't in the case of wood, see Section 3.4, the elastic models show that the amount of sink-in h_s is given by:

$$h_s = \varepsilon . \frac{P_{max}}{S} \tag{1}$$

where ε is a constant depending on the indenter geometry ($\varepsilon = 0,75$ for the measurement in this thesis), P_{max} is the maximum load and S is the elastic unloading stiffness.

From the Fig. 5 (right) it is obvious, that the contact between the material and the indenter is not along the whole measured depth, but it is necessary to subtract the amount of the sink-in. After that the contact depth is given by:

$$h_c = h_{max} - h_s = h_{max} - \varepsilon . \frac{P_{max}}{S}$$

(2)

where h_{max} is the maximum measured depth of the indentation and h_s is the amount of the sink-in of the material during the indentation [4].

Area function

The area function gives us the value of the projected contact area of the indenter tip. For a proper determination of the elastic moduli it is necessary to calibrate the area function carefully by independent measurements on a material with known properties (usually fused silica) to take the deviations from an ideal tip geometry into account. The area function used in the Hysitron® TI 750L Ubi™ for the indentation modulus computation is:

(3)

$$A = C_0 . h_c^2 + C_1 . h_c + C_2 . h_c^{1/2} + C_3 . h_c^{1/4} + C_4 . h_c^{1/8} + C_5 . h_c^{1/32}$$

where A is the area function (sometimes called the indenter shape function), C_x are calibration constants and h_c is the contact depth of the indenter given by the equation (2). The equation varies for different indenter tips and the number of members of the equation depends on the required accuracy of the computation [4].

Indentation modulus

The indentation modulus (also called reduced modulus) is the main variable quantified from the measured data, which describes the tested material resistance to being deformed elastically by the applied force. The equation considering isotropic indentation is given by:

$$E_r = \frac{\sqrt{\pi}}{2 . \beta} . \frac{S}{\sqrt{A}}$$

(4)

where E_r is the indentation modulus, β is the dimensionless parameter of the indenter tip geometry (β=1,034 used for the Berkovich indenter in the measurement evaluation), S is the measured elastic unloading stiffness $S=dP/dh$ and A is the area function [4].

<u>Sample Young's modulus</u>

The sample Young's modulus is the modified indentation modulus, which takes into account that the elastic material response could occur in both the specimen and the indenter tip. Utilizing material properties of both materials in the contact, the sample modulus is given by:

$$E_s = (1 - v_s^2) \cdot \left(\frac{1}{E_r} - \frac{1 - v_i^2}{E_i} \right)^{-1} \tag{5}$$

where E_s and v_s are Young's modulus and Poisson's ratio of the specimen, respectively and E_i and v_i are Young's modulus and Poisson's ratio of the indenter, respectively and E_r is the indentation modulus [4].

<u>Hardness</u>

Once the contact area is known, it is possible to determine the hardness by:

$$H = \frac{P_{max}}{A} \tag{6}$$

where P_{max} is the maximum load and A is the contact area. It is necessary to note that this equation is based on the contact area under load, so it may deviate from the traditional hardness measured from the area of the residual hardness impression, if the material exhibits a significant elastic recovery during unloading [4].

3.3 Sample preparation

The small pieces of the Norway spruce (1x1cm in cross section and 3 cm long, approximately) were cut from the timber, embedded in epoxy resin, placed into vacuum and left there for a while to eliminate an unwanted gas. Cured samples were cut with diamond cut-off wheel into 5 mm thick slices using water cooling. Then all samples were ground with silicon carbide grinding papers with grit 1200 grain/cm^2, 2400 grain/cm^2 and 4000 grain/cm^2 under water to eliminate thermal degradation of wood, using 2 minutes sequences of the grinding alternating with 5 minutes sequences of the drying on the air to prevent water soaking to the wood microstructure. Approximately 5 sequences for each paper were performed. After each grinding level, all samples were cleaned in an ultrasonic bath of drinkable water for 2 minutes,

approximately, to remove the loose particles of the ground material. As the last step of the sample preparation, the surface polishing on the Struers MD-Dac cloth with lubricant for water-sensitive materials was used to achieve the best surface as possible.
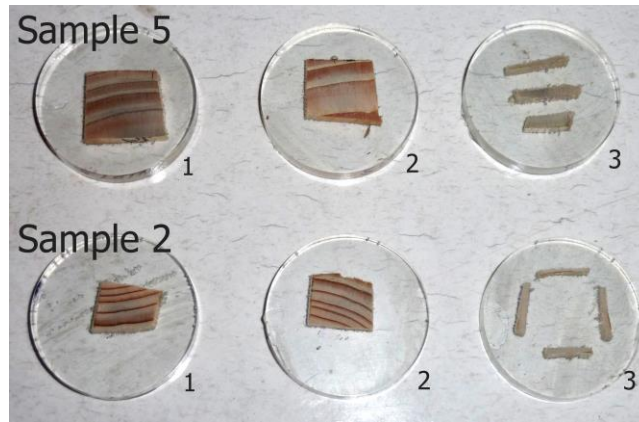

Fig. 6 Prepared samples for nanoindentation

3.4 Measurement

The static nanoindentation was performed using Hysitron$^®$ TI 750L Ubi$^™$ with diamond Berkovich tip (v_i=0,07, E_i=1141 GPa), as mentioned in the beginning of this section. All indentation points were located to the middle layer of the secondary wall – S_2 using the click script method for a proper selection of the indented area. The trapezoidal load function with the 10s hold period of the maximum force of 400 µN, and 5s for both loading and unloading with load-rate 80 µm/s, were used for all samples. For each indentation point, the load-displacement curve was plotted – all curves with a significantly different shape or with a wrong position of the indent were eliminated.

From measured data was computed indentation modulus E_r using Eq. (4) and afterwards Young's modulus employing Eq. (5) using Poisson's ratio of the sample (v_s=0,25) from micromechanical model mentioned in Section 4 and the material properties of the indenter (v_i=0,07; E_i=1141 GPa). The results of the indentation are summarized in Table 1 and Table 2, respectively.

Mean values of the indentation modulus E_r [GPa]			
	Sample 2	Sample 5	Samples 2+5
Earlywood	14.27	13.56	14.04
Transition zone	13.81	16.25	15.36
Latewood	13.90	16.36	14.84
Overall	13.94	16.21	14.87

Table 1: Mean values of the indentation modulus E_r

Mean values of the Young's modulus E_s [GPa]			
	Sample 2	Sample 5	Samples 2+5
Earlywood	13.55	12.86	13.21
Transition zone	13.40	15.45	14.59
Latewood	13.16	15.57	14.10
Overall	13.21	15.41	14.13

Table 2: Mean values of the Young's modulus E_s

There seems to be correlation between measured data and surface roughness. The sample 5 had a very rough surface and lower indentation modulus compared to sample 2. After re-polishing the surface became smoother and the indentation modulus significantly higher. Some measured data of the roughness and indentation modulus are given in Table 3 as an example. However, the surface of all samples remained rougher than desired, unless the great care was taken for the preparation. It would be better to prepare samples using an ultramicrotome (very sharp diamond knife), so the polishing and grinding would not be necessary.

Sample 5	RMS roughness [nm]	Indentation modulus E_r [GPa]
Before re-polishing	62.82	7.85
	87.37	9.74
After re-polishing	22.63	18.13
	32.45	18.01

Table 3: Measured data of the surface roughness and indentation modulus

It is necessary to note that in [4] the authors mention that great care must be taken if the h_f/h_{max} ratio is larger than 0,7 (h_f – the final depth, h_{max} – the maximum displacement, see Fig. 5). This ratio describes the behaviour of the tested material under pressure of the indenter tip, especially the pile-up of the material along the tip. High values of this ratio obviously lead to large errors in the contact area, which affects the hardness (the function of A, see Eq. (6)) and indentation modulus (the function of $\sqrt{A}$, see Eq. (4)). From values in Table 4 is evident that large errors for both tested samples might appear. The solution of this problem could be the direct measurement of the contact area from indentation scans or derivation of equation, which do not include the contact area. Unfortunately, the measurement of each contact area is almost impossible, at least very time-consuming, and it requires specific equipment for a proper scanning and a very long scanning time. The derivation of the equation not containing area function could be the focus of the future study.

The values of h_f/h_{max} ratio			
	Sample 2	Sample 5	Samples 2+5
Mean	0.70	0.74	0.71
Minimum	0.57	0.63	0.57
Maximum	0.81	0.84	0.84

Table 4: The values of the h_f/h_{max} ratio

4. Homogenization

4.1 Main principle

Wood is generally heterogeneous material. It is a natural composite consisting of many components, starting at atomic level. However, for the structural analysis we need only few values of the mechanical properties of the building material. In this case, it means that only properties of the whole timber are desired. For this purpose, it is necessary to implement homogenization model to get the effective value of the whole material, not only constructional parts. The main homogenization principle is based on substituting a heterogeneous material with a homogeneous material of equivalent properties. Although there are many methods of micromechanical homogenization, only two methods were used in this thesis. In particular, the Self-consistent method and the Mori-Tanaka method seem to be well suitable for our purpose.

Self-Consistent method

The Self-consistent method belongs to effective medium approximations based on a solution of an auxiliary inclusion problem. The interaction between inclusions is imagined by placing an inclusion into a homogeneous medium that has the overall effective properties. This method is well suitable for materials with almost the same volume fractions of phases, so the role of the matrix and inclusions could be reversed. Unfortunately, this method is implicit and leads to an iterative computation. In this thesis, the transformed version of the equation is adopted:

$$\frac{c_1.K_1}{3.K_1 + 4.G^{SC}} + \frac{c_2.K_2}{3.K_2 + 4.G^{SC}} + \frac{5}{3}.\left(\frac{c_2.G_1}{G^{SC} - G_1} + \frac{c_1.G_2}{G^{SC} - G_2}\right) + \frac{2}{3} = 0 \quad (7)$$

where c, K, G are the volume fraction, bulk modulus and shear modulus of each phase, respectively, and K^{SC} and G^{SC} are the homogenized bulk modulus and homogenized shear modulus, respectively [5].

Mori-Tanaka method

The Mori-Tanaka method belongs to effective field approximations. This method is based on a solution of a single inclusion in an unbounded matrix loaded by unknown average field in the matrix. The method is well suitable for a material with predominant matrix with some inclusions. Fortunately, the method provides explicit form so the computation is much easier and faster. Apart from the common formulation of the Mori-Tanaka method used for the second homogenization step, the transformed version of the equation is adopted in case of lumens (the third homogenization step). Considering properties of the inclusions equal to zero, the resulting effective properties of the homogenized material are given by:

$$k^{MT} = \frac{(1-f).k_1.m_1}{f.k_1 + m_1}$$

$$l^{MT} = \frac{(1-f).l_1.m_1}{f.k_1 + m_1}$$

$$n^{MT} = (1-f).n_1 + (l^{MT} - (1-f).l_1).\frac{l_1}{k_1} \tag{8}$$

$$m^{MT} = \frac{(1-f).k_1.m_1}{k_1 + f.(k_1 + 2.m_1)}$$

$$p^{MT} = \frac{1-f}{1+f}.p_1$$

where f is the volume fraction of pores, upper index $^{(MT)}$ means the effective properties of the homogenized material, lower index $_{(1)}$ describes properties of the matrix and k, l, n, m, p are given by:

$$k = -\left[\frac{1}{G_T} - \frac{4}{E_T} + 4\frac{v_A^2}{E_A}\right]^{-1}$$

$$l = 2.k.v_A$$

$$n = E_A + 4.k.v_A^2 = E_A + \frac{l^2}{k} \tag{9}$$

$$m = G_T$$

$$p = G_A$$

where E_A, G_A, v_A are the longitudinal Young's modulus, shear modulus and Poisson's ratio and E_T, G_T are the transversal Young's modulus and shear modulus, respectively [5].

4.2 Modification for wood

As it was said, the wood exhibits highly irregular microstructure, but it is possible to consider the microstructure as more or less regular. The type of the wood composition leads to the upscale homogenization, which could contain many steps. The three last steps (cell wall, earlywood/latewood, laminate) are depicted schematically on Fig. 7.
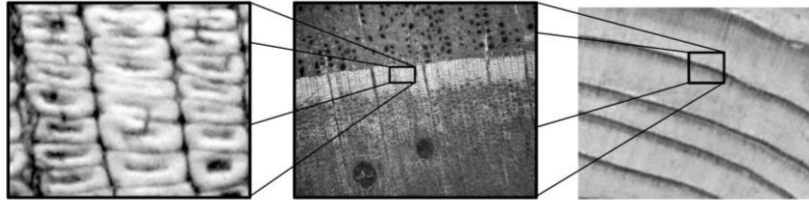

Fig. 7 The three last steps of the upscale homogenization

The micromechanical homogenization starts at the level called the polymer network with a characteristic length of a representative volume element (marked as RVE in the following text) in the range of 8-20 nm. The polymer network consists of hemicellulose, lignin, water and extractives, in this thesis the last two components (water + extractives) are neglected, so the volume fractions are given as:

$$f_{hemcell} + f_{lig} = 1 \tag{10}$$

where $f_{hemcell}$ and f_{lig} are the volume fractions of the hemicellulose and lignin respectively. Certainly, it is possible to start at the lower scales such as the atomic constitution of the cell walls, but it is too detailed and for our purpose it is not necessary. The hemicellulose and lignin have almost the same volume fractions and are mixed, so the Self-consistent method with spherical inclusions in the isotropic matrix seems to be well suitable for this homogenization step [6].

Following the cell wall composition, the next step adopts the polymer network from the previous step as a matrix supplemented with amorphous and crystalline cellulose as infinite cylindrical inclusions, because of the fibre-like origin of the celluloses, employing:

$$f_{polynet} + f_{crycell} + f_{amocell} = 1 \tag{11}$$

where $f_{polynet}$, $f_{crycell}$ and $f_{amocell}$ are the volume fractions of the polymer network, crystalline cellulose and amorphous cellulose, respectively. The characteristic length of RVE falls within the range of 0,5-1 μm. These assumptions lead to the Mori-Tanaka method for isotropic matrix with infinite cylindrical inclusions, which are parallel

to the longitudinal cell axis. The results of this step correspond to the effective properties of the cell wall, however with zero microfibril angle. The effective properties of the cell wall with non-zero microfibril angle will be mentioned later [6].

Further step provides the effective properties of the earlywood and latewood material. The homogenization model is made up of the cell wall forming the matrix and lumens as infinite hollow cylindrical inclusions, which are parallel to one another and also with the longitudinal cell axis, assuming that:

$$f_{cw} + f_{lum} = 1 \qquad (12)$$

where f_{cw} and f_{lum} are the volume fractions of the cell wall and lumens, respectively. The characteristic length of RVE for this step is in the range of 100-150 μm. The Mori-Tanaka method is used again in the same way as in the previous step, with only one difference, that the inclusions are pores so the stiffness is equal to zero, recall Eq. (8) [6].

The last step comprises of the laminate consisting of earlywood and latewood, considering that:

$$f_{EW} + f_{LW} = 1 \qquad (13)$$

where f_{EW} and f_{LW} are the volume fractions of the earlywood and latewood, respectively. The characteristic length of RVE is about 3-6 mm. The standard rule of mixture is used to obtain the Voigt and Reuss bounds of the effective Young's modulus employing equations:

$$L^{Voigt} = f_{EW}.L^{EW} + f_{LW}.L^{LW}$$

$$M^{Reuss} = f_{EW}.M^{EW} + f_{LW}.M^{LW} \qquad (14)$$

where f_{EW} and f_{LW} are the volume fractions of the earlywood and latewood, respectively, and L, M are the stiffness and compliance matrices, respectively. The index $^{(EW)}$ is for earlywood and $^{(LW)}$ is for latewood. The Voigt bound represents the upper value and the Reuss bound the lower value of the material properties [5].

In the whole computation the matrix member X_{33} represents the longitudinal direction of the cell walls. Considering transversely isotropic material the compliance matrix is given by Eq. (15), from which all Young's moduli, shear moduli and Poisson's ratios in both longitudinal and transverse directions were determined.

$$M = \begin{vmatrix} \dfrac{1}{E_T} & -\dfrac{\nu_T}{E_T} & -\dfrac{\nu_A}{E_A} & 0 & 0 & 0 \\[2mm] -\dfrac{\nu_T}{E_T} & \dfrac{1}{E_T} & -\dfrac{\nu_A}{E_A} & 0 & 0 & 0 \\[2mm] -\dfrac{\nu_A}{E_A} & -\dfrac{\nu_A}{E_A} & \dfrac{1}{E_A} & 0 & 0 & 0 \\[2mm] 0 & 0 & 0 & \dfrac{1}{G_A} & 0 & 0 \\[2mm] 0 & 0 & 0 & 0 & \dfrac{1}{G_A} & 0 \\[2mm] 0 & 0 & 0 & 0 & 0 & \dfrac{1}{G_T} \end{vmatrix} \tag{15}$$

In Eq. (15) E_A, G_A and ν_A are Young's modulus, shear modulus and Poisson's ratio in the longitudinal direction, respectively, and E_T, G_T and ν_T are Young's modulus, shear modulus and Poisson's ratio in the transverse direction, respectively.

4.3 Samples homogenization

<u>Step 1 – Polymer network</u>

Characteristic length of RVE: 8-20 nm

- Self-consistent method with spherical inclusions
- Two phases: lignin and hemicellulose
- Water and extractives are neglected

Input values:

	K [GPa]	G [GPa]	ν [-]	f [-]
Lignin	5.00	2.30	0.30	0.52
Hemicellulose	8.89	2.96	0.35	0.48

Table 5: The properties of the polymer network phases [6]

The input values were taken from [6] and modified for the case without water and extractives. The HELP program was used for the computation of the effective properties of the polymer network, using lignin as a matrix and hemicellulose as spherical inclusions employing the Self-consistent method. Both phases are assumed as isotropic materials, with values given in Table 5.

<u>Step 2 – Cell wall</u>

Characteristic length of RVE: 0,5-1 µm

- Mori-Tanaka method with infinite cylindrical inclusions
- Three phases: polymer network, crystalline cellulose, amorphous cellulose

– Microfibril angle is considered as zero

Input values:

	K [GPa]	G [GPa]	ν [-]	f [-]
Polymer network	-	-	-	0.61
Crystalline cellulose	-	-	-	0.22
Amorphous cellulose	5.56	1.85	0.35	0.17

Table 6a: The properties of the cell wall phases [6]

Polymer network (stiffness matrix)					
9.978	4.777	4.777	0	0	0
4.777	9.978	4.777	0	0	0
4.777	4.777	9.978	0	0	0
0	0	0	2.601	0	0
0	0	0	0	2.601	0
0	0	0	0	0	2.601

Table 6b: The properties of the cell wall phases

Crystalline cellulose (stiffness matrix)					
35.0	0	0	0	0	0
0	35.0	0	0	0	0
0	0	168.0	0	0	0
0	0	0	5.8	0	0
0	0	0	0	5.8	0
0	0	0	0	0	4.5

Table 6c: The properties of the cell wall phases (E_{33} corresponds to longitudinal axis) [6]

The values for the crystalline and amorphous cellulose were also taken from [6] and the effective properties of the polymer network from the previous step. For the computation was used the HELP program again, with polymer network as a matrix and crystalline and amorphous cellulose as infinite cylindrical inclusions parallel to the longitudinal axis, employing the Mori-Tanaka method. The amorphous and crystalline cellulose are supposed to be isotropic and transversely isotropic, respectively, whereas the polymer network is transversely isotropic.

Step 3 – Lumens

Characteristic length of RVE: 100-150 μm

– Mori-Tanaka method with infinite cylindrical inclusions

– Two phases: cell wall, lumens

– Microfibril angle is considered as zero

Input values:

	f_{lum} [-]	E [GPa]	G [GPa]
Earlywood	0.42	1E-200	1E-200
Latewood	0.18	1E-200	1E-200

Table 7a: The properties of the phases

Cell wall (stiffness matrix)					
11.600	5.094	4.107	0	0	0
5.094	11.600	4.107	0	0	0
4.107	4.107	44.360	0	0	0
0	0	0	2.910	0	0
0	0	0	0	2.910	0
0	0	0	0	0	2.741

Table 7b: The properties of the phases (E_{33} corresponds to longitudinal axis)

For this step it was necessary to find out the volume fractions of the lumens for both earlywood and latewood (Table 7a). The image analysis was used for this purpose, on Fig. 8 are two pictures as an example. On the left hand side is an original photograph from optical microscope, while on the right hand side there is a black-and-white picture used for the analysis of phase volume fractions. The image analysis was performed for each sample for both earlywood and latewood tracheids and the mean values of the volume fractions were obtained using the normal (Gaussian) distribution. The effective properties of the earlywood and latewood were predicted using the HELP program, with the cell wall as a matrix and lumens as infinite cylindrical inclusion parallel to the longitudinal cell axis, employing again the Mori-Tanaka method. Because the computation is not defined for zero values of elastic and shear modulus, the very small values near zero were presumed, see Table 7a.
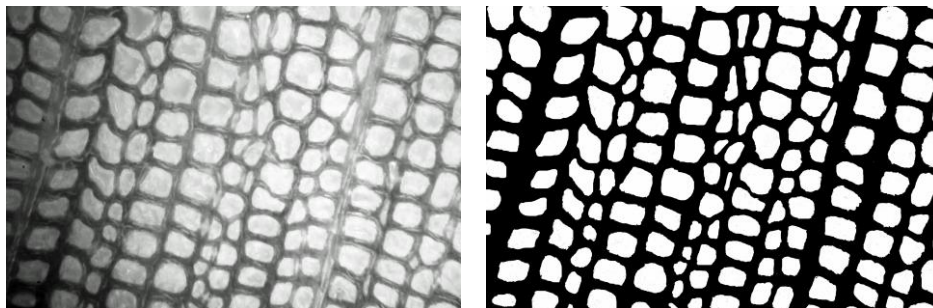

Fig. 8 The image analysis – Sample 2_1 earlywood

<u>Step 4 – Laminate</u>

Characteristic length of RVE: 3-6 mm

- − Standard rule of mixtures
- − Two phases: earlywood, latewood

Input values:

	f_{EW} [-]	f_{LW} [-]
Sample 2	0.79	0.21
Sample 5	0.50	0.50
Overall	0.67	0.33

Table 8: The volume fractions of the earlywood and latewood laminas

Earlywood (stiffness matrix)					
3.282	1.169	1.095	0	0	0
1.169	3.282	1.095	0	0	0
1.095	1.095	25.100	0	0	0
0	0	0	1.189	0	0
0	0	0	0	1.189	0
0	0	0	0	0	0.957

Table 9: The effective properties of the earlywood (E_{33} corresponds to longitudinal axis)

Latewood (stiffness matrix)					
6.548	2.556	2.240	0	0	0
2.556	6.548	2.240	0	0	0
2.240	2.240	35.820	0	0	0
0	0	0	2.022	0	0
0	0	0	0	2.022	0
0	0	0	0	0	1.751

Table 10: The effective properties of the latewood (E_{33} corresponds to longitudinal axis)

The image analysis was performed again to determine the volume fractions of the earlywood and latewood laminas. However, the measurement of the earlywood and latewood laminas is very inaccurate because of the indistinct boundaries of each lamina. More accurate would be to consider the whole growth ring. The mean values of the volume fractions were estimated using normal distribution again. The standard rule of mixtures was used for the computation, employing Eq. (9). The Voigt bound represents the upper estimation of the effective properties, while the Reuss bound represents the lower one.

Results:

	E_A [GPa]	G_A [GPa]	ν_A [-]	E_T [GPa]	G_T [GPa]	ν_T [-]
Polymer network	6.89	2.60	0.32	6.89	2.60	0.32
Cell wall	42.34	2.91	0.25	9.23	2.74	0.42
Earlywood	24.56	1.19	0.25	2.85	0.96	0.35
Latewood	34.72	2.02	0.25	5.50	1.75	0.38
Wood (Voigt)	27.91	1.46	0.25	3.72	1.22	0.36
Wood (Reuss)	27.18	1.38	0.25	3.38	1.13	0.35

Table 11: The effective properties of each step of the homogenization with zero microfibril angle

The values given in Table 11 are computed without influence of the microfibril angle (MFA=0°). The effective properties of the wood with a non-zero microfibril angle will be mentioned in Section 5.

5. Determination of microfibril angle

5.1 Microfibrils

The cell wall generally consists of cellulose, hemicelluloses, lignin and extractives. Lignin is an encrusting substance solidifying the cell wall, hemicelluloses are the matrix substances present between cellulose microfibrils. The cellulose occurs in the cell wall in the form of thin threads with an indefinite length, which are called cellulose microfibrils. The cellulose has crystalline nature, which is confirmed by many studies using e.g. X-ray diffractometry and polarization microscopy. The cellulose microfibrils consist of a core crystalline region of cellulose surrounded by paracrystalline cellulose and short-chain hemicellulose, while lignin encases them and binds them into a rigid structure of wood cell wall. The width of one cellulose fibre is in the range of nanometres, approximately 3,5 nm, and the cross section appears to be almost square. These microfibrils act in the cell wall like the steel reinforcement in a concrete and make a framework in the cell wall [3].

5.2 Microfibril angle

As it was said in Section 2.3 the microfibril angle (MFA) is defined as the deviation of the cellulose microfibrils in the cell wall from the longitudinal axis of the tree stem. MFA most probably depends on many factors. The first main factor is the position of the wood cell in tree stem. Many authors agree that MFA varies from pith to bark, being the highest in the pith, and differs with the height of the tree stem, being high

in the base of the stem, decreasing with height and increasing again near the top of the tree. Also the difference among trees has been observed in many studies, with the most obvious variation in the juvenile wood. Some authors found out the difference between the radial and tangential cell wall, but another authors report that there is no difference between them. The same diversity of the opinions could be seen in the case of the growth rate [7]. The dependence of MFA on the cell wall layer is mentioned in Section 2.3.

The relation between MFA and mechanical properties of the wood is obvious, especially for the stiffness. It has been shown that low MFA values result in a high longitudinal Young's modulus. This assumption is crucial for the computation in the next section. Adopting this idea, it is possible to make a reverse procedure and compute MFA using a comparison between the known elastic modulus taken from nanoindentation and the effective elastic modulus from micromechanical homogenization.

5.3 Direct measurement methods

Basically, there are two types of MFA measurement techniques: measurement of individual tracheids or fibres using microscopy, or measurement of bulk wood samples using X-ray diffraction or near infrared (NIR) spectroscopy. Some techniques are described below.

Polarisation microscopy

Polarised light microscopy belongs to the earliest techniques used to evaluate the microfibril orientation. Cellulose is partially crystalline, so thin sections of wood are birefringent when viewed between two crossed polarising filters. If the very thin longitudinal section is cut, it is possible to measure MFA as a weighted average of the whole secondary wall. The average microfibril angle is measured by rotating the tracheids or fibres until the bright cell wall becomes dark. This is called the maximum extinction position (MEP), where MFA is the deviation between the fibre axis and MEP. This method requires single cell wall preparation for the average MFA or the single cell wall layer preparation to determine MFA in each layer [7].

Direct visualisation using physical or chemical methods

These techniques are based on a surface fracturing, which produces coarse texture with microfibril clusters or lamellae that can be seen with a simple brightfield light microscope. One of the possible sample preparation is an iodine precipitation within

the cell wall. Iodine crystals form cavities in the cell wall and reveal the microfibrils, so it is possible to see them by microscope. However, it requires concentrated nitric acid, the fumes from which may damage the microscope equipment. Another preparation technique uses soft-rot to decay cavities in the cell wall so the microfibrils are visible. Unfortunately, it requires a long time for fungus to produce sufficient cavities (6-14 weeks). Also the mechanical fibrillation using ultrasonic treatment could be utilized, alone or in combination with chemicals [7].

<u>X-ray diffraction</u>

The X-ray diffraction can be employed when the sample is crystalline, fortunately the cellulose microfibrils are of the crystalline origin. MFA is obtained by measuring characteristics of the 002 equatorial reflection. This method belongs to the most popular ones [7].

<u>Infrared spectroscopy</u>

Near infrared (NIR) spectroscopy uses the near infrared region of the electromagnetic spectrum to scan the wood surface. Employing the prediction algorithm, it is possible to predict MFA [7].

5.4 Evaluation of MFA using nanoindentation data

Supposing that the cellulose microfibrils run helically around the cell wall (see Fig. 9 (left)) and MFA is defined within the plane tangential to the cell wall, there is no preferential plane containing longitudinal axis of lumens and the axis of the microfibrils. From that it is necessary to perform the orientation averaging before comparing both elastic moduli, to take into account all possible orientations of the microfibrils along the cell wall. The effective moduli at the cell wall level can be extracted from:

$$\langle\langle \boldsymbol{M^g} \rangle\rangle = \frac{1}{N} \sum_{i=1}^{N} \boldsymbol{M^g}\left(\alpha^i, MFA, 0\right) \tag{16}$$

$$\langle\langle \boldsymbol{L^g} \rangle\rangle = \frac{1}{N} \sum_{i=1}^{N} \boldsymbol{L^g}\left(\alpha^i, MFA, 0\right)$$

where N→∞ and $\boldsymbol{M^g}$, $\boldsymbol{L^g}$ are the compliance and stiffness matrices of the cell wall, respectively, transformed into the global coordinate system. In Eq. (16) α is the angle

which corresponds to the rotation about the longitudinal axis parallel to the direction of the lumens, i.e. the deviation of the plane, containing x_1 axis and microfibrils, from the x_2 axis, see Fig. 9 (right). It is also valuable to point out that in this case $\langle\langle M^g \rangle\rangle^{-1} \neq \langle\langle L^g \rangle\rangle$ in general [8].
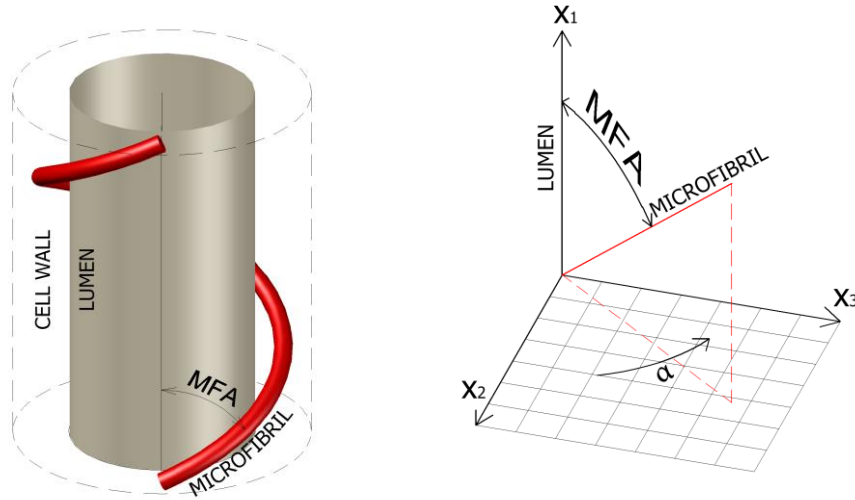

Fig. 9 Illustration of the microfibril angle

The process of finding MFA is iterative. However, the nanoindentation causes the off-axis loading so it is necessary to subtract the effective loading angle from the resultant angle to get the real MFA. The value of the loading angle 20° is assumed referred to [5].

For the comparison of the elastic moduli, the effective longitudinal modulus of the cell wall from the step 2 and the sample Young's modulus from nanoindentation were used. The results for both orientation averaging are summarized in Table 12.

	MFA [°]	
	Compliance averaging	Stifness averaging
Sample 2	7.91	21.27
Sample 5	4.08	18.13
Overall	5.12	19.95

Table 12: The values of the computed microfibril angle (MFA)

Employing again the micromechanical homogenization model we get the effective properties of the wood for both types of the orientation averaging. The results are summarized in Table 13 and 14. The homogenization procedure is the same as for the zero microfibril angle, with just one difference: the effective properties of the cell wall are

obtained by the fibre rotation and orientation averaging, which provides the transversely isotropic stiffness matrix used for the next homogenization steps.

	E_A [GPa]	G_A [GPa]	ν_A [-]	E_T [GPa]	G_T [GPa]	ν_T [-]
Polymer network	6.89	2.60	0.32	6.89	2.60	0.32
Cell wall	32.47	4.76	0.36	8.61	3.05	0.41
Earlywood	18.83	1.94	0.36	2.76	1.02	0.35
Latewood	26.62	3.31	0.36	5.24	1.90	0.38
Wood (Voigt)	21.40	2.39	0.36	3.58	1.31	0.36
Wood (Reuss)	20.85	2.25	0.36	3.27	1.21	0.35

Table 13: The effective properties of each step of the homogenization with MFA= 19,95° using the stiffness orientation averaging

	E_A [GPa]	G_A [GPa]	ν_A [-]	E_T [GPa]	G_T [GPa]	ν_T [-]
Polymer network	6.89	2.60	0.32	6.89	2.60	0.32
Cell wall	38.65	2.94	0.26	8.63	2.97	0.45
Earlywood	22.42	1.20	0.26	2.74	1.00	0.37
Latewood	31.69	2.04	0.26	5.22	1.86	0.40
Wood (Voigt)	25.47	1.48	0.26	3.56	1.29	0.38
Wood (Reuss)	24.81	1.39	0.26	3.25	1.18	0.37

Table 14: The effective properties of each step of the homogenization with MFA= 5,12° using the compliance orientation averaging

The resulting values of the effective properties are relatively high comparing to the literature [6], e.g. with values of the E_A in the range of 5,038-18,18 GPa, unlike Poisson's ratio which is lower. This inaccuracy is probably caused by the simplification of the homogenization model. There are several structural components which have been neglected, but might have a considerable impact on the final properties. For example, the rays which run radially in the wood stem decrease the longitudinal stiffness, while the radial properties increase. Also the resin canals, which act like wide hollow tubes, make the microstructure much weaker.

5.5 Other possible approaches of MFA determination

Another possible inverse approach of MFA evaluation is based on a comparison between the micromechanical prediction from homogenization and Young's modulus gained from indentation employing the Pilodyn 6J testing device. The Pilodyn measurement is based on a shooting of the indenter tip into the wood with a given energy and measuring the indentation depth while simultaneously controlling the wood moisture.

From the measured indentation depth could be simply computed macroscopic longitudinal elastic modulus E_A employing equation (17), which assumes that the indentation is performed in the transverse direction of the wood stem,

$$E_A = A + B.h \qquad (17)$$

where E_A is the longitudinal elastic modulus, A and B are constants determined statistically from the measured data, h is the penetration depth. Assuming the h [mm] and E_A [GPa] there are two groups of constants: the first group contain the original constants with values A = 19,367 and B = -0,5641, see [8], and the latter one are updated constants with values A = 17.41911236 and B = -0.2979367551, see [11]. The elastic modulus given by Eq. (17) is actually the value of the whole wood, so for the comparison we have to use the micromechanical prediction from the last step (laminate) of homogenization with a non-zero microfibril angle. For the prediction of the MFA, the Voigt bound and stiffness orientation averaging were used. The results are summarized in Table 15 and normal distribution of the elastic modulus computed by both equations is depicted in Fig. 10 with the mean value of MFA written next to the curve [8].

	Pilodyn test E [GPa]	Homogenization E [GPa]	Microfibril angle MFA [°]
Original equation	13.51	13.64	32
Updated equation	14.32	14.28	31

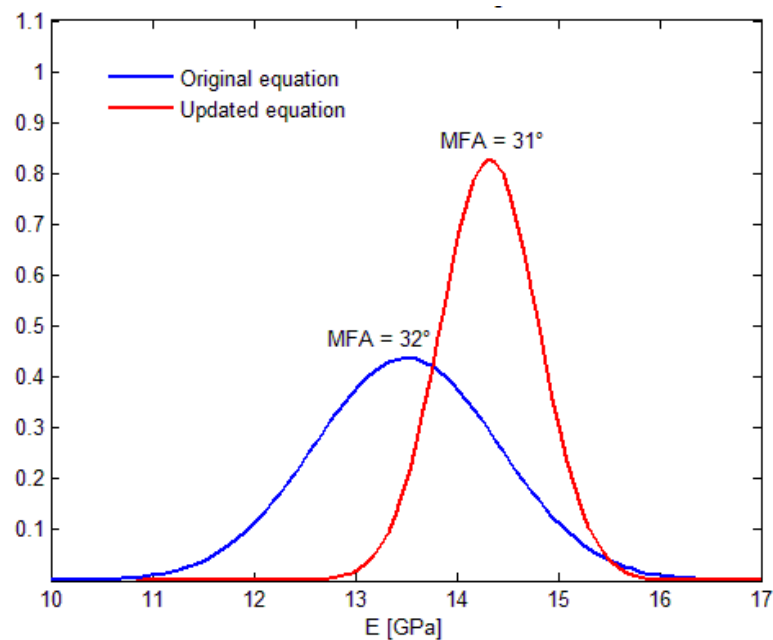Table 15: The values of the MFA from Pilodyn test

Fig. 10 The normal distribution of the Young's modulus from Pilodyn

Next approach, which is inverse too, uses comparison between the elastic modulus from the last homogenization step (laminate) and the modulus from tensile tests. As for the tensile tests, 17 samples were prepared as thin veneers with widening on both ends. The shape of the sample is visible on Fig. 11 with typical tensile failure after the test.

Fig. 11 The sample number 7 from the tensile test

The calculation procedure was the same as for the Pilodyn test, assuming the stiffness averaging and Voigt bound. The volume fractions of earlywood and latewood were gained from the image analysis using photographs taken by the scanning electron microscope (SEM). The resulting angles, see Table 16, are almost the same as from the Pilodyn test, except the last sample (n. 17), which has considerably smaller elastic modulus than other samples, probably caused by some microstructural inhomogeneities.

Sample n.	E [GPa]	Volume fractions		MFA [°]	E_{hom} [GPa]
		Earlywood	Latewood	Voigt	
1	9.5953	0.70	0.30	39	9.59
2	-	0.73	0.27	-	-
3	12.876	0.71	0.29	33	12.84
4	11.033	0.72	0.28	36	11.06
5	11.234	0.71	0.29	36	11.10
6	10.039	0.70	0.30	38	10.08
7	-	0.73	0.27	-	-
8	11.421	0.68	0.32	36	11.22
9	-	0.63	0.37	-	-
10	11.96	0.65	0.35	35	11.92
11	9.7536	0.62	0.38	39	9.87
12	11.714	0.65	0.35	35	11.92
13	-	0.76	0.24	-	-
14	11.246	0.71	0.29	36	11.10
15	13.061	0.67	0.33	33	13.03
16	13.043	0.62	0.38	33	13.26
17	6.2618	0.64	0.36	50	6.11

Table 16: The values of the MFA from tensile tests

However, both methods give significantly different estimates than that from nanoindentation. The reason of the differentiation between all presented methods might

be the subject of the future study. It is also important to note that authors in [1] mention that the value of the elastic modulus depends on the type and direction of loading and from that the elastic modulus from the compression test and tensile test is different.

6. Conclusion

For the proper use of the wood as a building material, it is necessary to understand the whole composition and material behaviour under loading in the building construction. This method would give a valuable notion of the influence of the particular wood components on the effective mechanical properties of the wood. Understanding the wood composition is still under development and is also a subject of many research studies.

The wood is generally anisotropic material with highly irregular structure, possibly determined as a fibre reinforced polymer composite. The main part of the tree used in the timber production is a stem. On the cross section of the tree stem are well visible growth rings which divide into earlywood and latewood. As many materials with biological origin, the wood consist of cells. Main wood mass comprises tracheids, possibly described as long closed tube-like cells with almost a rectangular cross section, elongated in the axial direction of the stem. The hollow space in the middle of the tracheid is called lumen and serve as a conductor of the water and nutrients. The most important load bearing components are tracheids, more accurate the cell walls. The main particles of the cell wall, with probably the highest strength, are cellulose fibres called microfibrils, which deviate from the longitudinal axis of the cell with an angle, named the microfibril angle (MFA). This angle is probably the reason of the strength deviation of different trees and also in the tree itself. Many studies confirmed that low MFA result into the high longitudinal modulus and with increasing MFA the elastic modulus is decreasing.

This dependence of MFA and longitudinal elastic modulus was utilized to estimate the value of MFA using comparison between the elastic modulus gained from the micromechanical homogenization and the known elastic modulus from the nanoindentation measurement. Upscale homogenization was used employing the Self-consistent method for the first step (Polymer network), the Mori-Tanaka method for the second (Cell wall) and third step (Lumens) and standard rule of mixtures for the fourth step (Laminate). The properties of each phase were taken from the literature [6] and some of the volume fractions were determined by image analysis, using pictures

mainly taken by optical microscope. Before the comparison it was necessary to employ the orientation averaging to take into account all possible orientations of the microfibrils along the cell wall. Two methods of the orientation averaging were employed – the stiffness averaging, which represents parallel connection of the components and lead to the Voigt estimation and the compliance averaging, which represents series connection and lead to the Reuss estimation.

As it was said, the microfibril angle has a great impact on mechanical properties. This is evident from Table 11, 13 and 14. Comparing these tables the fibre rotation decreases the value of the longitudinal elastic modulus, whereas the transversal elastic modulus is slowly increasing. The resulting microfibril angles: 5,12° for the compliance averaging and 19,95° for the stiffness averaging, lie in the range of 5-20° given in the literature [7]. The question is, which averaging gives the accurate value of the microfibril angle. The possible solution could be the implementation of the orientation averaging into the formulation of the Mori-Tanaka method. This approach lead to the similar values as from the stiffness averaging – Voigt estimation, whereas the compliance averaging – Reuss estimation give significantly different results. The comparison of all used methods is summarized in Table 17. For the confirmation of methods, it would be interesting to perform the direct measurement of MFA to find out if the theory approximates the reality using methods described in Section 5.3.

	$E_{longitudinal}$ [GPa]	MFA [°]
Isotropic nanoindentation		
Compliance averaging (Reuss)	24.81	5.12
Stiffness averaging (Voigt)	21.40	19.95
Mori-Tanaka averaging	32.60	19.89
Anisotropic nanoindentation (M-T)	25.07	28.06
Pilodyn (stiffness averaging)		
Original equation	13.51	32
Updated equation	14.32	31
Tensile test (stiffness averaging)	11.41[1]	36[1]
		[1] without sample n. 17

Table 17: Comparison between all used methods

In this study the great impact of the microfibril angle on mechanical properties was confirmed, however the micromechanical homogenization model still exhibits many inaccuracies such as neglecting of many structural components or transformation of the geometric shape of some components. One of the fundamental errors is

the modelling of the lumens as infinite hollow cylinders. The more exact model would be the prolate ellipsoids with flattened sides approaching the rectangular shape of the cross section. Also the perforation of the tracheid cell walls made by pit-pairs could be included in the model. Another important imperfection is neglecting of the rays and resin canals. The rays run radially and strengthen the wood structure in the radial direction, however weaken it in the longitudinal direction. The resin canals appear in the microstructure of the wood as large hollow tubes approaching the cylindrical shape and weaken the structure in both directions. There are also many macroscopic inhomogeneities such as knots, which have a great impact on the macroscopic properties, or ingrown bark or other imperfections. It might be worthy to separate the cell wall and the middle lamellae, which bonds cells together, and upgrade the micromechanical homogenization model.

The microstructural composition also plays an important role in the micromechanical homogenization. The volume fractions of each component differ a lot in the whole stem, so the consideration of the constant volume fractions can lead to a great error. There are many phenomena which could not be even noticed, such as the composition of the cell wall phases – the content of the cellulose, lignin etc. this can be improved only by a large statistical data set from particular laboratory tests. The same problem can occur in the case of the volume fraction of pores (lumens, rays and resin canals). The image analysis can distort the values and gives only the in-plane overview of the wood microstructure composition. In contrary, the comparison between the volume density of the whole sample and the matrix density of the cell wall, which is used by many authors, gives better results, however there is no notion about the types of the components, i.e. what portion of the overall porosity belongs to lumens etc.

	Overall porosity [-]
Image analysis	
Sample 2	0.344
Sample 5	0.308
Helium pycnometry	
Sample 2	0.443
Sample 5	0.550

Table 18: Comparison between two methods of the porosity determination

It is evident from Table 18 that the helium pycnometry gives higher porosity than image analysis. It is probably caused by neglecting of the other types of voids in the image

analysis, where only lumens were considered. However, wrong determination of the porosity can lead to great errors, such as overestimation of the elastic modulus, which might be considerably higher in the case of low porosity. The valuable method of attack seems to be the X-ray microtomography combined with XFEM which gives the overview of the whole wood composition. However, it requires specific equipment and knowledge.

Also the assumption of the homogeneous material (the isotropic half space) by means of the static nanoindentation might cause errors. Actually, the cell wall is not homogeneous and isotropic at all, so the anisotropic nanoindentation seems to be a reasonable solution. The results using the anisotropic approach are mentioned in Table 17 employing the orientation averaging implemented into the Mori-Tanaka method. Comparing anisotropic and isotropic evaluation of the nanoindentation employing the same orientation averaging (implemented in the Mori-Tanaka method), the isotropic approach gives higher Young's modulus and subsequently lower MFA, whereas the compliance and stiffness averaging provide almost the same values of the elastic modulus as anisotropic indentation, however with different MFA.

Another inaccuracy could occur during nanoindentation measurement due to the imperfect sample preparation. During cutting and grinding the wood might soak the water and dry again, this changing of the water content might damage the microstructure, and the water can extract some constituents of the wood structure. As well the movement of the grinding paper can destroy the microstructure. This would be reduced by the ultramicrotome cutting of the samples, which removes the grinding and polishing from the sample preparation process and so the water. Cut samples using ultramicrotome shows lower roughness compare to ground samples and there are no problems with water soaking and moisture content.

The static indentation may cause some inaccuracies due to the pile-up, which can be high in the case of wood, because of its viscoelasticity. This problem can be eliminated by employing the continuous stiffness measurement, which is usually used for the viscoelastic materials and might give better results.

Mentioned inaccuracies could be implemented in future studies to improve the measurement and estimation methods.

List of figures

List of tables

References

[1] Pentti O. Kettunen: *Wood – Structure and properties*; Enfield, N.H.: Trans Tech Publications Ltd., c2006. ISBN 978-087-8494-873

[2] [online] http://botanistbackyard.blogspot.cz/2012/05/plumbing-in-tree.html

[3] Minoru Fujita, Hiroshi Harada: *Ultrastructure and Formation of Wood Cell Wall*; Kyoto University, Kyoto, Japan (David N.-S. Hon, Nobuo Shiraishi: *Wood and cellulosic chemistry*. 2nd ed., rev. and expanded. New York: Marcel Dekker, c2001. ISBN 08-247-0024-4.)

[4] W. C. Oliver, G. M. Pharr: *Measurement of hardness and elastic modulus by instrumented indentation: Advances in understanding and refinements to methodology*; Journal of Materials Research, Vol. 19, No. 1, Jan 2004

[5] M. Šejnoha, J. Zeman: *Micromechanics in Practice*; Boston: WIT Press, c2013, ISBN 978-1-84564-682-0

[6] K. Hofstetter, C. Hellmich, J. Eberhardsteiner: *Development and experimental validation of a continuum micromechanics model for the elasticity of wood*; European Journal of Mechanics - A/Solids 24 (6), 2005, 1030-1053.

[7] L. Donaldson: *Microfibril angle: Measurement, variation and relationships – a review*; IAWA Journal, Vol. 29 (4), 2008: 345-386

[8] L. Melzerová, L. Kucíková, T. Janda, M. Šejnoha: *Estimation of orthotropic mechanical properties of wood based on non-destructive testing*; Wood Research. 2016, vol. 2016, ISSN 1336-4561

[9] The Forest Management Institute, Czech Republic (http://www.uhul.cz)

[10] Lesy České republiky, s.p., 2015 (http://www.lesycr.cz)

[11] M. Šejnoha, T. Janda, L. Melzerová, V. Nežerka: *Stochastic model of laminated timber beam*; Engineering Structures, submitted May 2016